IAC-21-C1-9-11

Attitude determination and control system testbed for hardware and software testing and verification for HYPSO small satellites

Jørgen Anker Olsen[a,1], **Mariusz Eivind Grøtte**[b,1], **Jan Tommy Gravdahl**[c,1]
[1] *Department of Engineering Cybernetics, Norwegian University of Science and Technology, Trondheim, Norway*
[a]*jorgen.a.olsen@ntnu.no,* [b] *mariusz.eivind.grotte@ntnu.no,* [c] *jan.tommy.gravdahl@ntnu.no*

Abstract

In recent years, there has been a significant increase in the number of small satellites that have been developed and launched into Low-Earth-Orbit (LEO), herein utilizing suited commercial-off-the-shelf components and further lowering the development and production costs. Attitude Determination and Control System (ADCS) is a critical ingredient to ensure survivability and successful operations of small-satellites and their payloads, communications, and other subsystems. This paper presents the design, development and construction of an ADCS testbed dedicated, but not limited to, for testing full-scale ADCS components for Cube-satellites built at the Norwegian University of Science and Technology (NTNU), such as HYPSO-1 (HYPer-spectral SmallSat for ocean Observation) and SelfieSat by Orbit NTNU. The ADCS testbed can also be used by other interested parties in academia and the aerospace industry, and the technical drawings and specifications will be available for all interested parties.

The ADCS testbed will be primarily used for a) characterization of small-satellite reaction wheels, magnetorquers and attitude sensors; b) calibration of small-satellite attitude sensors such as magnetometers, sun sensors, gyroscopes and accelerometers; c) development and performance testing of attitude control and estimation algorithms. The testbed enables a quasi-frictionless simulated environment with software-adjustable magnetic field model, sun emulation, and a spherical air-bearing. To generate a uniform and time-varying local magnetic field represented in-orbit, a $2 \times 2 \times 2$ m^3 Helmholtz cage has been constructed which can be controlled directly from an operator through a microcontroller. The magnetic field of the Helmholtz cage can be controlled in software based on adjustable orbital elements, an IGRF model and local calibration, or subtraction, with respect to the Earth's magnetic field. Furthermore, the spherical air bearing makes it possible to carry out actuation and/or sensor tests in quasi-frictionless rotational motion with 3 degrees of freedom, constrained only by ±25 deg in pitch and roll.

Theory, calculations, and simulations have been used throughout to verify construction, approaches, and results. The testbed has also been successfully demonstrated for performance characterization in detumble and sun sensor tests for a full 2U CubeSat. The testbed is planned to test parts for the upcoming HYPSO-2 and -3 satellites.

1. Introduction

There has recently been a tremendous rise in popularity and utility of small satellites [1], mainly due to their low weight, affordability and alleviated complexity when compared to the traditional large satellites. A CubeSat, often categorized as a micro- or nanosatellite, is typically built with one or more standardized 10 cm × 10 cm × 10 cm (1U) elements (cubes). This standardization, together with reduced costs in the project life-cycle, use of commercial off-the-shelf (COTS) components, and less complex electronics, computers, and communications, has been particularly appealing for commercial businesses and universities [2].

The versatility and reliability of COTS-based systems for small satellites has increased, many regularly being proven with flight heritage. This, combined with targeted operational testing of subsystems during the pre-launch phase, has widely boosted the success rate of CubeSat missions [3]. Moreover, with the pressing customer demands also the number and variety of suitable COTS components keep growing, although seldom having been flight-proven with tailored functionality in an integrated satellite system. This mandates facilities that enable rigorous characterization, calibration, and qualification testing of such —especially applicable to the Attitude Determination and Control System (ADCS) which accommodates control and estimation algorithms that mutually depend on a wide array of actuators and sensors in real time.

This paper describes an ADCS testbed constructed at the

Norwegian University of Science and Technology (NTNU), mainly by the impetus to enable characterization and calibration of ADCS hardware and functional testing of software for the HYperspectral small-Satellites for Ocean observation (HYPSO) developed at the NTNU Small Satellite Laboratory [4]. It consists of a Helmholtz cage, a BeagleBone microcontroller for controlling magnetic field, an air bearing, a sun emulator, and a modular self-built test-platform that may host several ADCS components, or whole CubeSats. Upon assembly and Helmholtz cage calibration, the testbed was used for detumbling a SelfieSat Engineering Model (EM), a 2U CubeSat developed by the student organization Orbit NTNU.

This paper is organized as follows. Section 2 presents the functional and design requirements for the ADCS testbed. In Section 3 the details on design, construction and assembly of the testbed are described. Section 4 presents experimental results for model verification, and magnetic field characterization and calibration of the Helmholtz cage, and results from detumbling test of SelfieSat. The results are discussed in Section 6 and conclusions are provided in Section 7.

2. Methodology

2.1. *Overview*

The main goal for the ADCS testbed is to imitate the key force sources and attitude reference points in Low-Earth-Orbit (LEO) to enable realistic characterization and calibration of ADCS components and to test algorithms developed for attitude estimation and control in real time. The design requirements are summarized in a Table 1, being partially based on existing functional testbeds, e.g. [5], [6], [7], and [8].

The overall structure of the ADCS testbed consists of: a) a Helmholtz cage generating a magnetic field that encompasses a test subject at its center; b) a height-adjustable stand with an air bearing at the center of the cage, here defined as the test-stand; and c) a weight-adjustable rigid plate, hosting various sensors and actuators or smaller CubeSats, that shall float on top of the air bearing, here defined as the test-platform; and d) a sun emulator providing a sun vector which, in addition to magnetometer measurements inside a Helmholtz cage, enables greater accuracy in attitude determination. The definition of "testbed" here refers to all elements a), b), c), d) and any other apparatus required to operate it, i.e. power supplies, electronics, microcontrollers, operator-PCs and software. The testbed shall be designed to host at least a 3U $\times$ 2U (6U) CubeSat model.

Table 1 Design Requirements for ADCS Testbed.

No.	Requirement
1.	The ADCS testbed shall host a CubeSat with dimensions of at least 3U $\times$ 2U (6U).
2.	The ADCS testbed shall emulate the Earth's magnetic field in LEO.
3.	The Helmholtz cage shall maintain a magnetic field with magnitude of at least 250 μT.
4.	The Helmholtz cage shall produce a homogeneous magnetic field within a reference volume of 50 cm $\times$ 50 cm $\times$ 50 cm around the geometric center.
5.	The magnetic field strength within the reference volume of the Helmholtz cage shall not deviate by more than 4%.
6.	The magnetic field strength within the reference volume of the Helmholtz cage shall not deviate by more than 3% each in x-, y-, and z-axes.
7.	The ADCS testbed shall emulate free fall.
8.	The ADCS test-stand shall be height-adjustable.
9.	The center of mass and inertia of the test-stand shall be adjustable.
10.	The ADCS test-platform shall host magnetometers, sun sensors, inertial measurement units, magnetic torquers, and momentum wheels.
11.	The ADCS test-platform shall be modular with the possibility of changing and mounting multiple sensors and actuators.
12.	The test-platform shall be mounted on top of an air-bearing.
13.	The test-platform shall freely rotate about local inertial z-axis (yaw).
14.	The ADCS testbed shall emulate the position of the Sun in LEO.

2.2. *Requirements for the Magnetic Field*

A major element of the testbed is to replicate a variable magnetic field at any location in LEO, where the magnitude can reach up to 100 μT [9]. The solution is to utilize a Helmholtz cage consisting of three electromagnetic coil pairs placed in an orthogonal triad configuration. For the best representation of Earth's magnetic field in LEO, the

Helmholtz cage needs to calibrate for the local one and the smaller interference from electrical components. The magnetic field also needs to be uniform over a sufficiently large region, here chosen not to deviate by more than 4% at a 25 cm distance from the geometric center, i.e. a reference volume of 50 cm × 50 cm × 50 cm. Moreover, external power supplies are needed to safely provide the required current to the coils to generate the desired magnetic field strength.

2.3. *Requirements for Rigid Body Rotation*

The testbed shall emulate free fall in orbit and enable rotation of a rigid body about one axis using torques from e.g. magnetic torquers and/or reaction wheels. This is realized by using an air bearing to lift the test-platform to balance the Earth's gravitational force. The test-platform is placed on top of the air bearing, and needs to be safely secured so that it does not tip over while hovering.

In addition, a solution of having a monofilament line suspending a test subject into the Helmholtz cage center, also enables adequate but limited attitude control using magnetic torquers. This is useful if magnetic torquers are too weak to handle the additional inertia added by the test-platform on the air bearing.

2.4. *Requirements for the Sun Emulator*

A sufficiently strong light source, e.g. a lamp or flashlight, shall provide an emulated inertial sun vector to the test subject hosting sun sensors and running attitude estimation algorithms. The sun vector is found by normalizing the light intensity into three components defined in an inertial or body reference frame.

3. Theory

3.1. *Magnetic Field*

The magnetic field for a pair of Helmholtz coils can be calculated with Biot-Savart's law. Following the derivation in [5], [8] and [10], the magnetic field d$\mathbf{B}$ generated by a current I passing through a wire length d$\mathbf{l}$ is given by

$$\mathrm{d}\mathbf{B} = \frac{\mu_0}{4\pi} \cdot I \frac{\mathrm{d}\mathbf{l} \times \hat{\mathbf{r}}}{r^2}, \tag{1}$$

where μ_0 is the magnetic permeability, r is the distance between the wire segment and the measurement point of magnetic field, and $\hat{\mathbf{r}}$ is the unit vector along the wire segment.

The total magnetic field around the coils may be found by calculating the field generated by one single coil side of length L, and applying super-positioning. Given a magnetic field $\mathbf{dB_t}$ along the z-axis, and by integrating (1), the magnetic field generated by one side along the z-axis becomes

$$\begin{aligned}\mathbf{B}_{\text{side}}(z) &= \int \mathbf{dB_t} \\ &= \frac{\mu(NI)}{4\pi} \int_{-L/2}^{L/2} \frac{(L/2)dx}{(z^2 + (L/2)^2 + x^2)^{3/2}} \hat{\mathbf{z}}, \end{aligned} \tag{2}$$

where N is the number of coil windings and $\hat{\mathbf{z}}$ is a unit vector along the locally defined z-axis. The integral in (2) is evaluated using

$$\int \frac{dx}{(a^2 + x^2)^{3/2}} = \frac{x}{a^2\sqrt{a^2 + x^2}}, \tag{3}$$

and therefore the magnitude of the magnetic field generated by one side of the coil is

$$B_{\text{side}}(z) = \frac{\mu NI}{\pi} \cdot \frac{L^2}{(4z + L^2)\sqrt{4z^2 + 2L^2}}. \tag{4}$$

Multiplying (4) by four and adding the field generated by the other coil pair, the resulting magnetic field generated by a coil pair is

$$B(z)_{\text{total}} = 4B_{\text{side}}(z_A) + 4B_{\text{side}}(z_A - D), \tag{5}$$

where D is the distance between the coils. This can be rewritten for the special case if the center of the coil pair is considered, i.e. $z_A = D/2$, resulting in

$$B(z_A)_{\text{total}} = \frac{8\mu NI}{\pi} \cdot \frac{1}{\left((D/L)^2 + 1\right)\sqrt{(D/L)^2 + 2}}. \tag{6}$$

To achieve uniformity in the magnetic field and for best efficiency, the optimal spacing between the coils D_{optimal}, according to [5], should be

$$D_{\text{optimal}} \triangleq \gamma_{\text{optimal}} \cdot L = 0.5445L, \tag{7}$$

where $\gamma_{\text{optimal}} = 0.5445$ is the optimal spacing factor.

3.2. *Simulations of Magnetic Field*

Simulations were performed to obtain the desired size and homogeneity of the magnetic field in the 50 cm × 50 cm × 50 cm reference volume surrounding the center of the Helmholtz cage. Two cases of simulations were performed: one specifically using (4)–(6) in Matlab; and the second using COMSOL Multiphysics. The COMSOL simulation was modeled with electromagnetic coil parameters given in Table 2, for which 25 different configurations were investigated to

obtain the optimal parameters with regard to the size of the cage and coils, number of coil windings, strength of current, and spacing between the coils.

The International Geomagnetic Reference Field generation 13 (IGRF-13) model was used to generate the magnetic field as experienced in LEO. The IGRF model uses empirical data to calculate the magnetic field strength the x-, y-, and z-axes of a local North-East-Down (NED) frame or Earth-Centered-Inertial (ECI) frame [11]. Due to the Earth's magnetic field turning with the Earth's rotation, the local NED-frame is considered as inertial [12]. For a Helmholtz cage creating a IGRF-based magnetic field at a specified point in orbit, the actual magnetic field on the Earth's surface must be subtracted. The local magnetic field also affects the calibration of Helmholtz cage and individual components that are subject for testing, which is also compensated for by subtraction.

3.3. *Detumbling*

Detumbling aims to reduce and stabilize the spin of a satellite, especially after deployment from a launcher in the Launch and Early Operations Phase (LEOP). While the satellite is idle it may potentially attain excessively high angular velocity, leaving only the magnetometers as the available attitude sensors and thus making initial attitude determination difficult while the satellite is booting. With their low power consumption, the primary actuators typically used for detumbling are magnetic torquers. In this case, these utilize the local magnetic field to generate counter-acting and platform-stabilizing torques.

An established method for detumbling is the b-dot algorithm [12], [13]. The b-dot control law, expressed in body frame (superscript "b"), is given by

$$\mathbf{m}^b = -k\dot{\mathbf{B}}^b - \mathbf{m}_c, \tag{8}$$

where $\mathbf{m}^b$ magnetic dipole moment generated by the coils, $\dot{\mathbf{B}}^b$ is the differential of the Earth's local magnetic field vector, and the $\mathbf{m}_c$ term dissipates the kinetic energy. The magnetic torque required is given by

$$\boldsymbol{\tau}^b = \mathbf{m}^b \times \mathbf{B}^b. \tag{9}$$

4. Design, Construction and Assembly

4.1. *Helmholtz Cage Structure*

The Helmholtz cage size, copper thread diameter, number of windings for each coil, and amount of current were parameterized to find the best trade-off solution. The ideal design, that collectively optimize the strength and uniformity of the magnetic field for a given current, are listed in Table 2 and with the corresponding 3D CAD model design in SolidWorks shown in Fig. 1. Fig. 2 shows an x-z slice of the magnetic field strength across the center of the cage with its gradient displayed in the column bar to the right.

Table 2 Final structural design for the Helmholtz cage.

Parameter	**Value**
Copper thread diameter	2 mm
X-coils side length	1.9 m
Y-coils side length	1.95 m
Z-coils side length	2 m
# X-coils windings	30
# Y-coils windings	31
# Z-coils windings	32

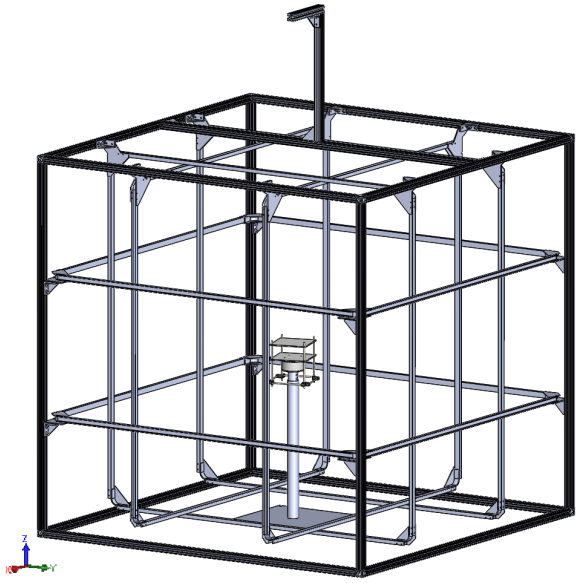

Fig. 1 SolidWorks 3D CAD model of the Helmholtz cage, with air bearing test-stand and -platform in center and mounting point for monofilament line at the top of the cage.

The cage was constructed using aluminium scaffolding as support structure to keep the coils in place, whereas the coils were made out of aluminium U-profiles. Screws, bolts, washers, and brackets were made of non-ferrous metals such as aluminum, brass or plastics. Fig. 3 shows the assembled Helmholtz cage with external scaffolding holding the three orthogonal coil pairs.

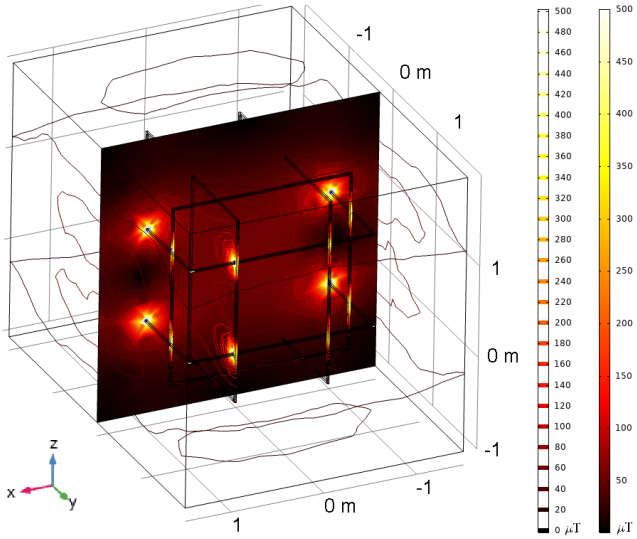

Fig. 2 An x-z slice and contour of the magnetic field density norm obtained in COMSOL for the Helmholtz cage coils.

Fig. 3 Assembled Helmholtz cage with two coils per axis.

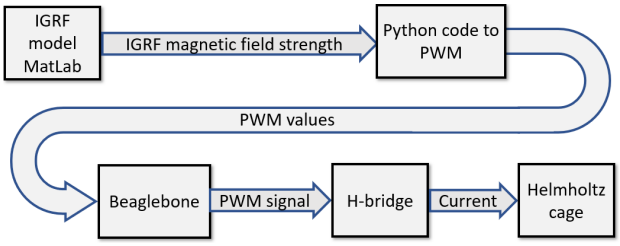

Fig. 4 Block diagram of the signal flow from the IGRF magnetic field values to the physical current going through the coils in the Helmholtz cage.

4.2. *Controlling the Magnetic Field*

Another trade-off study was performed to determine suitable power supplies for the different configurations of the Helmholtz cage, test-stand and available electronic components (i.e. power supply, H-Bridge, microcontrollers, and sensors). A total of six P1535 power supplies from Peak-Tech were selected, each providing current to one coil pair [14]. The current to the Helmholtz cage is controlled by a BeagleBone Black microcontroller coil with the polarity and strength being further adjusted by six Cytron DC Motor Driver H-bridges. The BeagleBone provides WiFi communications to the PC-operator to reduce any electromagnetic interference and to avoid cabling that hinder the test-platform rotation on the air bearing.

The magnetic field generated in the Helmholtz cage was controlled by the signals, segmented as depicted in Fig. 4. The information flow starts with an IGRF model in Matlab which is exported to Python. The BeagleBone Python script then uses a model of the Helmholtz cage to convert the magnetic field vector to pulse-width modulation (PWM). The PWM control signals are transmitted to H-bridges that control the current strength and polarity from the power supply. Finally, the current is sent to the Helmholtz coils to generate the desired IGRF-based magnetic field model.

4.3. *Air Bearing*

The air bearing, having a hemispherical shape with 60 mm radius and 39 mm depth, is dedicated for free rotation of a test-platform around at least one axis using a reaction wheel, similar to a satellite performing a slew maneuver. Moreover, the air bearing is designed to accompany a wide range of test subjects but are required to be mounted on a plate. The center of mass of the test-platform must be properly adjusted to coincide with the principal vertical axis of the air bearing where the air flow is most uniform. The air bearing is almost friction-less, although it is theoretically limited by a maximum mass of 60 kg at which significant static friction occurs. The pneumatic setup of the air bearing is illustrated in Fig. 5 and the completed test-stand with air bearing is shown in Fig. 6.

4.4. *Sun Emulator*

An Iiglo flashlight is chosen as the sun emulator, generating up to 11 600 lumen with a beam-width of 40°. The flashlight has five brightness settings and can be positioned at a distance between 0.2–2 m away from the test-stand. For a fixed setting, the distance can be appropriately adjusted to

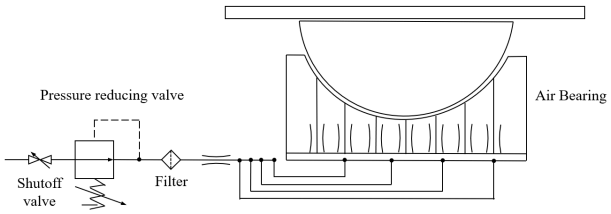

Fig. 5 Pneumatic diagram of air bearing illustrating from high pressure side on the left to low pressure on the right.

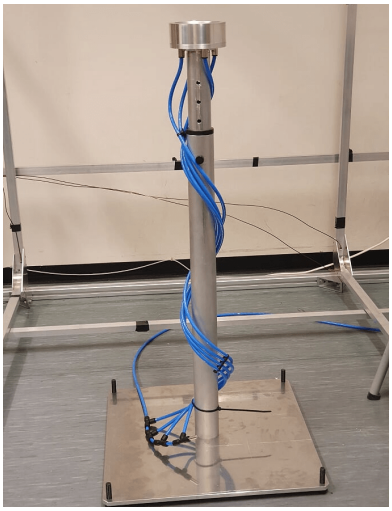

Fig. 6 Test-stand and air bearing with adjustable height function and pressure hoses attached.

choose a brightness in the range 1 000–250 000 lux [15].

4.5. *Test-Platform*

The test-platform is built by two acrylic plates connected with four brass threaded rods. It has a weight-and-balance system where mass increments may finely adjust inertia and align the center of mass so that the test-platform safely rotates on the air bearing. The complete test-stand with the Helmholtz cage, air bearing, sun emulator, and test-platform can be seen in Fig. 7.

The nominal test-platform serves as a readily available suite of sensors and actuators, i.e. being a standalone mock-up ADCS system. It is designed to accommodate gyroscopes, magnetometers, IMUs, sun sensors, magnetic torquers, and reaction wheels. It also includes batteries, a micro controller, and a WiFi-node, thus abstaining from using cables that physically hinder free rotation on the air bearing. The current array of sensors are a LSM303DLHC magnetometer, a MPU-6050 gyroscope, a TSL2591 light sensor, and a STIM210 IMU. Actuator system consists of a SatBus MTQ magnetorquer from NanoAvionics, and a self-manufactured 50 mm diameter aluminum reaction wheel accompanied by a Maxon EC 20 flat brushless DC electric motor with Hall sensors. Fig. 8 shows the reaction wheel being center-mounted on the top plate of the test-platform, and the BeagleBone and sensors on the lower plate.

The sensors and actuators can easily be removed if a whole CubeSat is the test subject. If that is the case, then the lower plate of the test-platform may be fitted with a tailored CubeSat-mount to ensure that it is properly balanced, aligned and secured on top of the air bearing. The CubeSat mount is modular and allows standard sizes from 1U to 12U. Fig. 9 shows the SelfieSat EM attached to the CubeSat mount while illuminated by the sun emulator for sun vector determination and sun sensor characterization.

Fig. 7 Complete ADCS testbed with the test-platform balancing, but safely secured, on top of the air bearing.

4.6. *Test Solution for Detumbling a CubeSat*

Using magnetic torquers for detumbling a CubeSat in short time is not optimal on the air bearing unless the magnetic field strength of the Helmholtz cage is set to be significantly larger than that found in LEO. This is due to mainly three reasons: the modest torque generated by a magnetic torquer, a small dynamic friction of the air bearing, and the significantly larger combined inertia of the CubeSat and test-platform. Reaction wheels, on the other hand, create sufficiently larger torques and should be able to resolve the

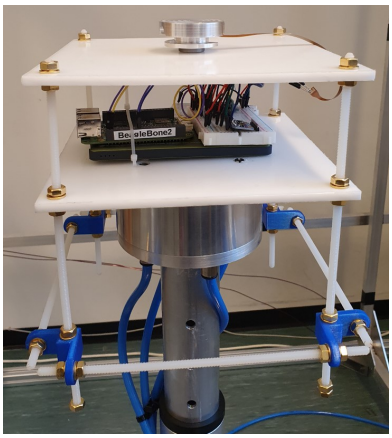

Fig. 8 Reaction wheel, BeagleBone and sensors mounted on the test-platform.

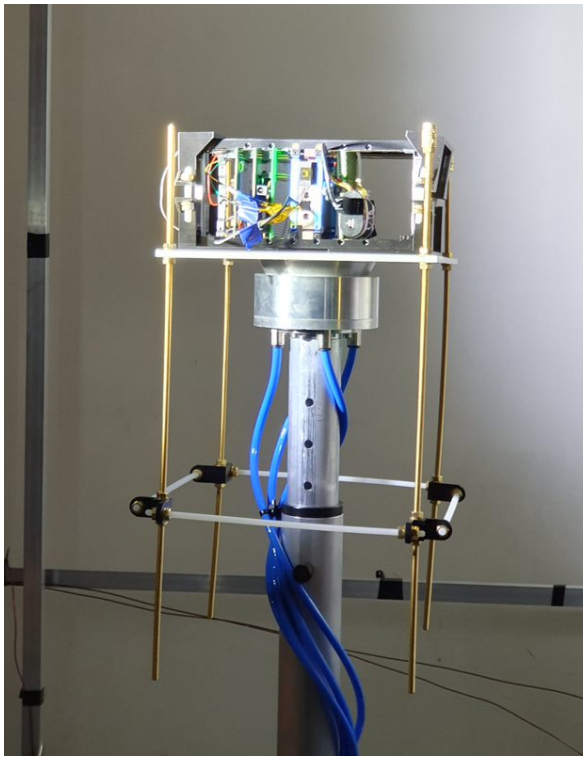

Fig. 9 SelfieSat EM attached to the CubeSat mount and hovering over the air bearing during sun vector determination.

problem, as discussed in [14]. Hence, for detumbling, a monofilament line is used instead of the air bearing which has almost no additional mass nor friction.

5. Experimental Results

5.1. *Characterization of Helmholtz Cage*

The Helmholtz cage was set to run with 1 A and 2.5 A current at 1.25–3.3 V to verify its capability to attain the desired magnetic field strength and uniformity inside the 50 cm × 50 cm × 50 cm reference volume. The measurements were compared against simulation results in Matlab and COMSOL, and the calculations using (6). The comparison is shown in Fig. 10, where measured values correspond well with Matlab simulations and theoretical calculations by at most 8.3% and 8% deviation, respectively, but are somewhat off compared to the results obtained in COMSOL with the highest discrepancy being 25% along the y- and z-axes for both 1 A and 2.5 A currents.

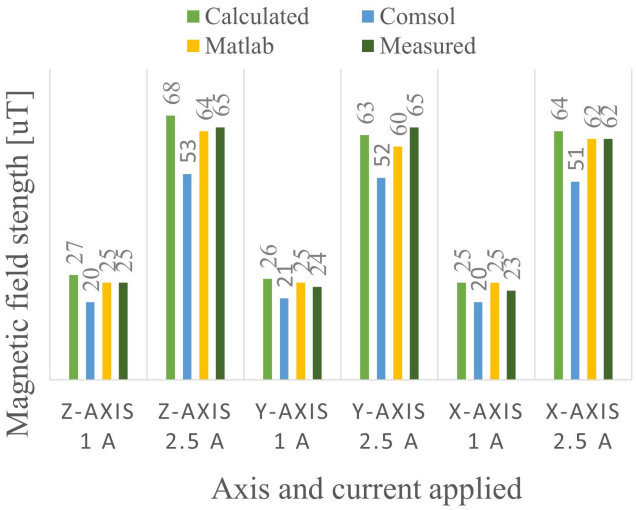

Fig. 10 Magnetic field strength comparison for coil pairs along x-, y-, and z-axes.

To determine the degree of uniformity, a magnetometer was used to measure the magnetic field along x-, y-, and z-axes for coil current of 2.5 A, shown in Fig. 11. The deviations along x-, y-, and z-axes are shown in Table 3, which indicates discrepancy of up to 12.0% at 50 cm distance from the center when compared with at most 2.9% at the boundary of the reference volume.

If needed, the cage is also capable of generating much stronger magnetic fields, up to 500μT in each axis by increasing the current applying to each coil in the coil pair to 20 A.

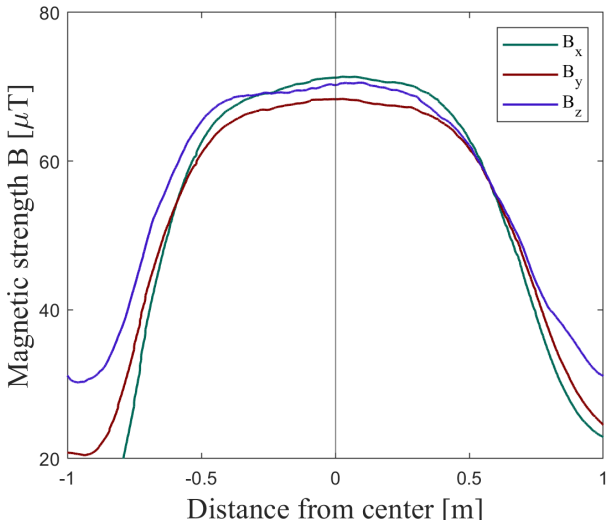

Fig. 11 Magnetic field measurements from center of Helmholtz cage, for all axes.

Table 3 Uniformity calculations and measurements. $B(z)_c$ is the measured magnetic field strength at the center of the cage. Units are given in μT.

Axis	$B(z)_c$	25 cm	50 cm	25 cm	50 cm
x	71.2	69.1	62.7	2.9%	12.0%
y	68.3	66.9	61.4	2.0%	10.1%
z	70.2	69.2	62.5	1.4%	11.0%

5.2. *Calibration for the Local Magnetic Field*

Calibrating the Helmholtz cage is required to replicate the IGRF-based magnetic field found at a location in a particular orbit. The Helmholtz cage was programmed to replicate the measured Earth's magnetic field in the background, but inducing opposite current directions in an attempt to cancel it. This test was performed for one axis at a time for five seconds with a two-second break in-between, followed by activating all of the coils simultaneously. The results can be seen in Fig. 12, where the Earth's magnetic field is almost completely cancelled between 32 and 37 seconds for all x-, y-, and z-axes.

Next, the IGRF-based magnetic field was generated by the Helmholtz cage for a 500 km altitude polar orbit with orbital elements defined in Table 4. Fig. 13 shows the simulated magnetic field at a particular true anomaly (here a range between -180 to 180 degrees) and the one generated by the Helmholtz cage. The largest deviation in magnetic strength between the IGRF model and generated magnetic field is 2.5μT.

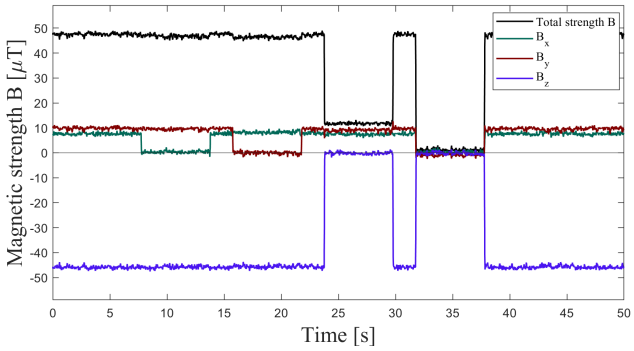

Fig. 12 Cancellation of the Earth's local magnetic field, one axis at the time for 5 second intervals, and all axes between 32 and 37 seconds.

Table 4 Orbital elements used in the Matlab IGRF model.

Orbital Element	**Value**
Semi-major axis	6870 [km]
Eccentricity	0.0 [-]
Inclination	90 [deg]
Right ascension of ascending node	0 [deg]
The argument of perigee	0 [deg]
True anomaly	0 [deg]

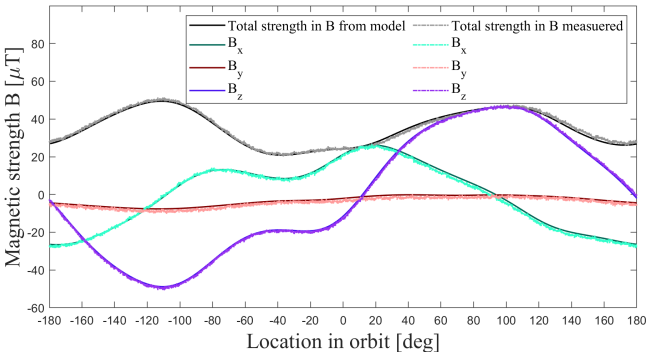

Fig. 13 Helmholtz cage magnetic field measurements and IGRF-based magnetic field at particular true anomaly (location of satellite in orbit).

5.3. *2U CubeSat Detumbling*

The SelfieSat EM was chosen as test subject for detumbling. It has a mass of 0.55 kg and is readily equipped with ADCS components such as three magnetic torquers, two magnetometers, a gyroscope, and an accelerometer. The CubeSat was attached to the monofilament line suspended from an aluminium strut and into the center of the cage,

enabling rotation about its vertical axis, as shown in Fig. 14. Next, the Helmholtz cage was programmed to generate the orbit-simulated magnetic field with the parameters in Table 4. The measured angular velocity of the CubeSat is shown in Fig. 15 for active (top) and non-active (bottom) b-dot detumbling.

Fig. 14 SelfieSat EM safely suspended into the Helmholtz cage center using a monofilament line.

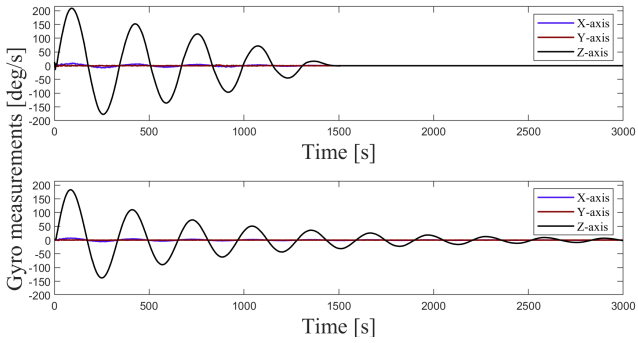

Fig. 15 Angular velocity of the SelfieSat EM during detumbling test with the b-dot detumbling algorithm being active in the top plot and inactive in the bottom plot.

6. Discussion

Upon validating the magnetic field generated by the Helmholtz cage, it has been demonstrated that theoretical calculations correspond well with the actual measurements with a maximum deviation of 8%, slightly better than the Matlab model, but much better than that in COMSOL with maximum deviation of 25%, as indicated in Fig. 10. However, gathering more statistical data from independent tests would be needed to give a more conclusive comparison.

The uniformity of the magnetic field, shown in Fig. 11 and Table 3, has measured to have an accuracy of 2.9% in a 50 cm $\times$ 50 cm $\times$ 50 cm envelope, therefore complying with the testbed design requirements. Increasing the volume to 100 cm $\times$ 100 cm $\times$ 100 cm resulted in a maximum uniformity deviation of 12%, which is too large, and manifesting the importance of placing test subjects more or less at the cage center for better use of magnetometers and magnetic torquers.

For emulating the magnetic field in orbit using the parameters Table 4, indicates good correspondence between the IGRF-model and the one calibrated and generated by the Helmholtz cage with maximum deviation of 2.5 μT, shown in Fig. 13. Although this is quite accurate, regulating the Helmholtz cage using direct measurements from magnetometers may further increase the accuracy as most of the deviation likely occurs if there there is a small drift in the generated magnetic field strength.

A CubeSat detumbling test, with a monofilament solution, has been successfully demonstrated as shown in Fig. 15, reducing the time for stabilizing the spin from about 3000 seconds (without) to 1550 seconds using the b-dot detumbling algorithm. For similar CubeSat tests on an air bearing, then greater torques (i.e. reaction wheels) and/or larger magnetic torquers would be required to handle the increased inertia of a combined CubeSat and test-platform.

7. Conclusions

The increasing interest and demand for small satellite missions, often as dedicated CubeSat projects at universities and in the commercial industry, requests readily available testing facilities to verify and validate the critical operational functions and systems. To support local small satellite projects, an ADCS testbed has therefore been constructed at the Norwegian University of Science and Technology. During the development and operational phases for a CubeSat, the testbed shall generally facilitate characterization of typical CubeSat-tailored ADCS sensors, and actuators, and assess the performance of chosen or prototyped attitude estimation and control algorithms.

To imitate the conditions in orbit, the testbed is chosen

to consist of a Helmholtz cage for generating a uniform IGRF-calibrated magnetic field; a monofilament line suspension for validating detumbling functions; an air bearing to enable controlled yaw rotation with reaction wheel(s); and a sun emulator for sun sensor characterization and a more complete validation of attitude estimation algorithms in real time. With the artificial magnetic field replicating that found in Low-Earth-Orbit, it is possible to perform realistic attitude control using CubeSat-tailored magnetic torquers and magnetometers. Detumbling within the magnetic field generated from the Helmholtz cage has been successfully demonstrated for the SelfieSat Engineering Model, a 2U CubeSat developed by Orbit NTNU.

Future work on the test-platform is planned to enable more rapid and accessible testing of ADCS components and algorithms, including: creating a graphical user interface for controlling the Helmholtz cage; completing the test platform sensor suite and actuators, and regulating the Helmholtz cage using direct measurements from magnetometers being permanently fixed to the test-stand.

Acknowledgement

The authors thank Orbit NTNU for collaboration and making their 2U CubeSat Engineering Model available for testing, and Bjørn A. Kristiansen, Terje Haugen, and Glenn Angel for their invaluable help with the construction of the ADCS testbed. This work was supported by the Research Council of Norway, Equinor, Det Norske Veritas (DNV) and Sintef through the Centers of Excellence funding scheme, Grant 223254—Center for Autonomous Marine Operations and Systems (AMOS) and the Research Council of Norway through the IKTPLUSS programme grant 270959 (MASSIVE).

References

[1] H. Polat, J. Virgili-Llop, and M. Romano, Survey, Statistical Analysis and Classification of Launched CubeSat Missions with Emphasis on the Attitude Control Method, Journal of Small Satellites, Volume 5, pages 513-530, 2016.

[2] M.N. Sweeting, Modern Small Satellites-Changing the Economics of Space, Proceedings of the IEEE, volume 106, number 3, pages 343-361, 2018.

[3] T. Villela, C. Costa, A. Brandão, F. Bueno, and R. Leonardi, Towards the Thousandth CubeSat: A Statistical Overview, Int. J. of Aerospace Engineering, pages 1-13, 2019.

[4] M.E. Grøtte, R. Birkeland E. Honoré-Livermore, S. Bakken, J. L. Garrett, E.F. Prentice, F. Sigernes, M. Orlandić, J.T. Gravdahl, T.A. Johansen, Ocean Color Hyperspectral Remote Sensing With High Resolution and Low Latency–The HYPSO-1 CubeSat Mission, IEEE Transactions on Geoscience and Remote Sensing, pages 1–19, 2021, DOI: https://doi.org/10.1109/TGRS.2021.3080175.

[5] R.C. da Silva, I.S.K. Ishioka, C. Cappelletti, S. Battistini and R. A. Borges, Helmholtz cage design and validation for nanosatellites HWIL testing, IEEE Transactions on Aerospace and Electronic Systems, 2019.

[6] S. Chesi, O. Perez, and M. Romano, A dynamic, hardware-in-the-loop, three-axis simulator of spacecraft attitude maneuvering with nanosatellite dimensions, J. Small Satell, Volume 4, pages 315-328, 2015.

[7] M. Prinkey, CubeSat Attitude Control Testbed Design: Merritt 4-Coil per axis Helmholtz Cage and Spherical Air Bearing, AIAA Guidance, Navigation, and Control (GNC) Conference, pages 4942, 2013.

[8] D.S. Batista, F. Granziera, M.C. Tosin, and L.M. de Melo, IEEE Transactions on Aerospace and Electronic Systems, Three-Axial Helmholtz Coil Design and Validation for Aerospace Applications , 2018 , 54, 1, pages 392-403, DOI: 10.1109/TAES.2017.2760560.

[9] J. Matzka, A. Chulliat, M. Mandea, C.C. Finlay, E. Qamili, Geomagnetic Observations for Main Field Studies: From Ground to Space, Space Science Reviews, Volume 155, pages 29 - 64, 2010.

[10] D.J. Griffiths, Introduction to electrodynamics; 4th edition, Pearson, 2013, Re-published by Cambridge University Press in 2017, DOI: 1108420419.

[11] J.J. Love, Magnetic monitoring of Earth and space, American Inst. of Physic, Physics Today, Vol 61, no 2, p. 31, 2008.

[12] J.T. Gravdahl, E. Eide, A. Skavhaug, K. Svartveit, K.M. Fauske, F.M. Indergaard, Three axis Attitude Determination and Control System for a picosatellite: Design and implementation, Proceedings of the 54th International Astronautical Congress, volume 7, 2003.

[13] R. Wisniewski, Satellite Attitude Control Using Only Elecromagnetic Actuation, Ph.D. thesis, Dept. of Control Engineering, Aalborg University, Denmark, 1996.

[14] J.A. Olsen, Attitude Determination and Control System Testbed for Hardware and Software Testing and Verification for Small Satellites, Master's thesis, Dept. of Engineering Cybernetics, Norwegian U. of Science and Tech., 2021.

[15] R. Volpe, J. Balaram, Technology for robotic surface inspection in space, Conference on Intelligent Robots in Factory, Field, Space, and Service, pages 1193, 1994.